Transactions of the Materials Research Society of Japan 34[4] 631-638 (2009)

X-ray specular and off-specular reflection from a protein adsorbed at a liquid surface

Yohko F. Yano[1], Tomoya Uruga[2], Hajime Tanida[2], Hidenori Toyokawa[2], Yasuko Terada[2], Masafumi Takagaki[2], and Hironari Yamada[3]
[1]Research organization of Science & Engineering, Ritsumeikan University,
1-1-1 Noji-Higashi, Kusatsu-shi, Shiga, 525-8577 Japan
Fax: 81-77-561-2680, e-mail: y-yano@fc.ritsumei.ac.jp
[2]Japan Synchrotron Radiation Research Institute, 1-1-1 Kouto, Sayo, Hyogo 679-5198 Japan
[3]Department of Photonics, Ritsumeikan University

X-ray specular and off-specular reflection was investigated to analyze the out-of-plane and in-plane structures of a globular protein adsorbed at an air/water interface in the presence of a salt. The x-ray reflectivity was used to obtain the electron density profile normal to the surface. The electron density profile indicates the presence of a double layer consisting of a lower-density lysozyme layer below a densely packed top layer. From the off-specular diffuse scattering, the protein layer could be well described by a simple exponentially decaying height–height correlation function with a correlation length of 500 Å. This suggests that the protein molecules aggregate and form islands on the water surface. A simple formula for describing the off-specular excess scattering above the capillary wave fluctuation was proposed to explain the lateral fluctuation of an inhomogeneous layer above a liquid surface.
Key words: x-ray reflectivity, off-specular diffuse scattering, PILATUS, air/water interface, lysozyme

1. INTRODUCTION

X-ray reflection is a powerful tool for investigating the structure of buried interfaces. It can be used to obtain the density profile normal to the surface with a subnanometer spatial resolution. By carefully examining diffuse scattering in the vicinity of specular reflection peaks, structural information parallel to the surface, namely the height–height correlation function, can also be obtained [1].

The surface morphology of liquid surfaces is governed by thermally excited capillary waves with molecular-size amplitudes and micrometer-order wavelengths [2]. Sinha *et al*. have theoretically demonstrated that diffuse scattering from liquid surfaces diverges algebraically at the specular reflection angle, creating large tails that extend into the surrounding off-specular region [3]. This theoretical prediction has been verified experimentally for simple molecular liquids [4–8] and liquid metals [7–10]. In contrast, scattering that exceeds the predicted capillary contribution has been observed for Langmuir monolayers on a water surface [11–14]. Fukuto *et al*. proposed a sum rule for scattering from an inhomogeneous layer on a liquid surface [12]. They used a simple exponentially decaying correlation function to describe the height–height correlation function of a Langmuir monolayer and they derived the correlation length and the surface roughness.

However, x-ray off-specular diffuse scattering measurements have been less popular than x-ray reflectivity measurements for the following reasons:

1. A system with a high angular resolution is necessary to detect the diffuse scattering intensity.
2. The scattered intensity is much weaker than the x-ray reflection.
3. The structural information is derived using a complicated fitting procedure and is rather ambiguous.

We recently developed a liquid interface reflectometer at SPring-8 [15, 16]. This reflectometer is equipped with a two-dimensional single x-ray photon counting pixel array detector (PILATUS) and can achieve an x-ray reflectivity of nearly 10^{-9} with an integration time of only 1 s at each angle, exhibiting enormous potential for rapid measurements. Previously, time-resolved measurements with a time resolution of 3 min were performed for the adsorption of a globular protein on an air/water interface [17].

In the present study, we exploit the advantages of the two-dimensional PILATUS detector to investigate both the x-ray specular reflection and the off-specular diffuse scattering intensities to analyze the out-of-plane and in-plane structures of a globular protein (lysozyme) adsorbed at an air/water interface. We also propose a simple formula for describing the diffuse scattering from an inhomogeneous protein layer on a water surface.

2. GRAZING INCIDENCE X-RAY SCATTERING TECHNIQUES

2.1 Liquid interface reflectometer

X-ray reflectivity measurements were performed using a liquid interface reflectometer developed at the BL37XU beamline of SPring-8 [15, 16]. Brilliant undulator radiation at 15 keV (λ = 0.826 Å) was used as the x-ray source; it had horizontal beam width of 50 μm. A single x-ray photon counting pixel detector, PILATUS [18, 19], with an area of 487×195 pixels (172 μm/pixel) was located 538 mm from the center of the sample. The

integration time at each incident angle was 1 s. Each pixel of PILATUS contains a charge-sensitive amplifier, a shaper amplifier, a single level discriminator and a 20 bit counter. The counting rate capability depends on the time constant of shaper amplifier, which is about 100 nsec in this experimental setup. This condition allows to detect up to 10^5 counts/pixel/s within the dead time of 1%. A set of aluminum sheets with a thickness in the range 1–6 mm was employed as an attenuator at the incident angle $\alpha < 0.9°$ to prevent the counting rate exceeding 10^5 counts/pixel/s. The scattering geometry is illustrated in Fig. 1. The incident wave vector $\mathbf{k}_{in}$ strikes the liquid surface at an incident angle α. The scattered x-rays are characterized by the output wave vector $\mathbf{k}_{out}$, which makes an angle β to the surface and an angle 2θ to the plane of incidence. The Cartesian components of the wave vector transfer $q = \mathbf{k}_{out} - \mathbf{k}_{in}$ are defined as:

$$\begin{aligned} q_z &= k\left[\sin(\alpha)+\sin(\beta)\right] \\ q_x &= k\cos(\beta)\sin(2\theta) \\ q_y &= k\left[\cos(\beta)\cos(2\theta)-\cos(\alpha)\right] \end{aligned} \quad , \qquad (1)$$

where $k = 2\pi/\lambda$. The typical FWHMs of the reflection profile at the incident angle α of 0.01° projected on the detector are 1.5 pixels horizontally (i.e., parallel to the x-axis) and 2.0 pixels vertically (i.e., parallel to the z-axis), which are related to reciprocal-space resolutions through $\Delta q_x \sim k\,\Delta(2\theta)$ and $\Delta q_y \sim k\,\sin(\beta)\Delta\beta$.

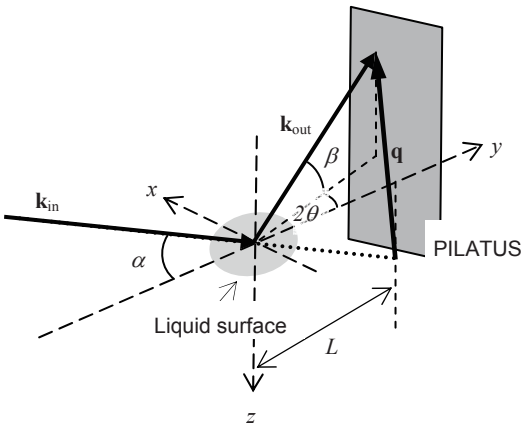

Fig. 1 X-ray scattering geometry. Incident wave vector $\mathbf{k}_{in}$ strikes the liquid surface at an incident angle α. The scattered x-rays are characterized by the output wave vector $\mathbf{k}_{out}$, which makes an angle β to the surface and an angle 2θ to the plane of incidence. The scattering intensity is detected by PILATUS, which is located L = 538 mm from the center of the liquid surface.

2.2 X-ray specular reflectivity

In the specular reflection condition, the reflectivity is measured as a function of q_z when $q_x = q_y = 0$, or equivalently $\beta = \alpha$ and $2\theta = 0$. Figure 2 shows a typical image around a reflection peak detected by PILATUS. Since this reflection peak was detected over five pixels horizontally, we considered the intensity measured five pixels from the center of the peak to be background. A reflection profile $I(z)$ was obtained by summing the signal intensities and subtracting the background as:

$$\frac{I(z)}{I_0} = \frac{1}{I_0}\left\{\sum_{|x|\le 3} I(z,x) - \frac{1}{2}\left[I(z,x=-5)+I(z,x=+5)\right]\right\} \qquad (2)$$

The total signal intensity corresponding to the first term in Eq. (2) and the background corresponding to the second and third terms are shown in Fig. 3. The reflection profile over a range of four orders of magnitudes was obtained after the background subtraction.

The reflectivity is calculated by summing the reflection profiles around the peak region of 13 pixels and normalizing this value with the intensity of the incident beam, which was monitored using an ionization chamber [15].

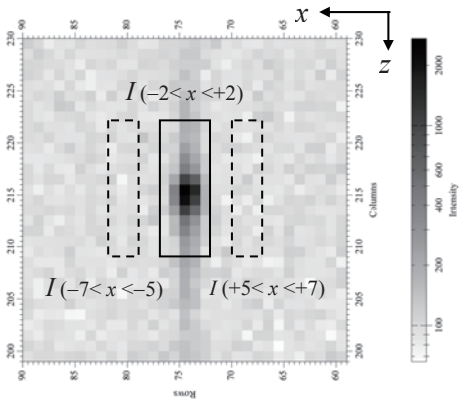

Fig. 2 Enlarge picture of an x-ray specular reflection image on PILATUS. Each square corresponds to a pixel with dimensions of 172 μm × 172 μm.

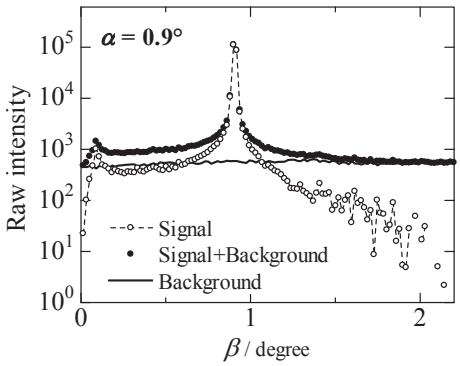

Fig. 3 Integrated signal, integrated background and integrated signal plus background for a reflection profile at $\alpha = 0.9°$.

The x-ray specular reflectivity for liquid surfaces is described by the Born approximation [7, 20]:

$$R(q_z) = R_F\left|\Phi(q_z)\right|^2 CW(q_z,T,\gamma) \quad , \qquad (3)$$

where R_F is the Fresnel reflectivity for an ideally flat interface and $\left|\Phi(q_z)\right|^2$ is the intrinsic structure factor normal to the surface, which is expressed as:

$$\left|\Phi(q_z)\right|^2 = \left|\frac{1}{\rho^{Bulk}}\int dz\,\frac{\partial\langle\rho(z)\rangle_{xy}}{\partial z}\,e^{iq_z z}\right|^2 \quad , \qquad (4)$$

where $\langle\rho(z)\rangle_{xy}$ is the lateral average electron density profile. $CW(q_z, T, \gamma)$ is the surface roughness term due to capillary waves and is given by:

$$CW(q_z, T, \gamma) = \exp(-\sigma_{cw}^2 q_z^2), \quad (5)$$

with

$$\sigma_{cw}^2 = \left(\frac{k_B T}{2\pi\gamma}\right)\ln\left(\frac{q_{\max}}{\Delta q_y}\right),$$

where γ is the surface tension, $q_{\max}$ is the upper cutoff for capillary contributions, which is determined by the condition that the number of capillary wave modes is of the order of the number of molecules per unit surface area; this is equivalent to fixing $q_{\max} \sim 2\pi/d$, where d is on the order of the intermolecular distance. Δq_y is the instrumental resolution of $\Delta q_y \sim k \sin(\beta)\Delta\beta$, where $\Delta\beta$ is related to the number of pixels summed to calculate the reflectivity as 13 pixels × 0.172 mm/pixel / 538 mm.

2.3 X-ray off-specular diffuse scattering

In off-specular diffuse scattering, the scattering intensity is measured at non-specular conditions: $\alpha \neq \beta$, or equivalently q_x, $q_y \neq 0$. A β-scan method, in which the scattered intensity is measured as a function of β at constant α has typically been conducted independently of x-ray reflectivity measurements. In the present study, we used the reflection profile normalizing with the peak intensity of the reflection profile at the incident angle α of 0.01°, which was assumed to be equivalent of the incident beam intensity I_0, as the off-specular diffuse scattering intensity.

The normalized intensity I/I_0 is generally equal to the convolution of the differential cross section $d\sigma/d\Omega$ with an appropriate instrumental resolution function Ξ:

$$\frac{I(q)}{I_0} = \int \frac{d^2 q'_{xy}}{k^2 \sin(\beta)} \Xi_q(q_{xy} - q'_{xy}) \frac{1}{A_0}\frac{d\sigma}{d\Omega}(q'_{xy}) \quad . \quad (6)$$

$$\Xi_q(\delta q_x, \delta q_y) = \begin{cases} 1 & \text{if } |\delta q_x| \le \Delta q_x/2, |\delta q_y| \le \Delta q_y/2 \\ 0 & \text{otherwise} \end{cases}.$$

The differential cross section for a homogeneous liquid surface is described by the capillary wave model [2,7] and can be written as:

$$\frac{1}{A_0}\left(\frac{d\sigma}{d\Omega}\right)_{hmg} \approx \frac{1}{16\pi^2}\left(\frac{q_c}{2}\right)^4 \frac{T_F(\alpha)T_F(\beta)}{q_z^2 \sin(\alpha)} \quad , \quad (7)$$
$$\times |\Phi_0(q_z)|^2 \frac{2\pi\eta}{q_{xy}^2}\left(\frac{q_{xy}}{q_{\max}}\right)^\eta$$

for $\eta = (k_B T/2\pi\gamma)\, q_z^2 < 2$, where A_0 is the cross-sectional area of the incident beam, q_c is the critical vector, and $T_F(\alpha)$ is the Fresnel transmission factor [1]. The scattering from a homogeneous liquid surface is described by the characteristic power law $1/q_{xy}^{2-\eta}$ of capillary-wave thermal diffuse scattering.

Fukuto *et al*. established a sum rule for scattering from capillary fluctuations on liquid surfaces [12]. If an inhomogeneous film (in which the local electron density deviates from the lateral average electron density profile $\langle\rho(z)\rangle_{xy}$) is formed on a liquid surface, additional scattering is superimposed on the diffuse scattering:

$$\frac{1}{A_0}\left(\frac{d\sigma}{d\Omega}\right)_{inhmg} \approx \frac{1}{16\pi^2}\left(\frac{q_c}{2}\right)^4 \frac{\phi_2^2 e^{-\sigma_2^2 q_z^2}}{\sin(\alpha)} \quad ,$$
$$\times \frac{1}{(2\pi)^2}\int_{q'_{xy}\le q_{\max}} d^2\mathbf{q}'_{xy} \frac{2\pi\eta}{q'^2_{xy}}\left(\frac{q'_{xy}}{q_{\max}}\right)^\eta C_2(\mathbf{q}_{xy} - \mathbf{q}'_{xy}) \quad (8)$$

where ϕ_2 is the average electron density ratio of the film to the bulk phase, σ_2 is the root-mean-square roughness of the film/gas interface, and C_2 is the Fourier transform of a simple exponentially decaying height–height correlation function $c_2(r_{xy}) = \sigma_2^2 \exp(-r_{xy}/\xi)$:

$$C_2(q) = \frac{2\pi\sigma_2^2\xi^2}{\left(1+\xi^2 q^2\right)^{\frac{3}{2}}} \quad , \quad (9)$$

with a correlation length ξ.

3. MATERIALS

The globular protein, lysozyme (LSZ), is elliptical in shape with approximate dimensions 30×30×45 Å^3. It is regarded as a rigid molecule due to the presence of four disulphide bridges. LSZ was selected because its three-dimensional conformation is very stable in solution and its adsorption behavior has been extensively studied [21–25]. Previously, time-resolved x-ray reflectivity measurements were performed for LSZ adsorbed at a air/water interface to investigate the mechanism of adsorption-induced protein unfolding [17]. The time dependence of the density profile at the air/water interface revealed that the molecular conformation changed significantly during adsorption. In the present study, we focus on the adsorption process in the presence of a salt.

3×crystallized and lyophilized hen egg lysozyme was purchased from Sigma (Prod. No. L6876) and used as supplied. Protein solutions were made using a phosphate buffer solution (0.02 M NaH_2PO_4/Na_2HPO_4) of pH 7 (ionic strength: 0.02 M) using UHQ-grade water. Protein solutions were made to concentrations of 43 mg/mL, from which 1 cm^3 portions were added to a 42 cm^3 buffer solution with 2 M NaCl in a Langmuir trough to give final concentrations of 1 mg/mL.

4. RESULTS AND DISCUSSION

4.1 X-ray specular reflectivity

The reflectivity data were divided by the Fresnel reflectivity of the buffer solution and the capillary wave contribution $CW(q_z, T, \gamma)$ given by Eq. (5). The intrinsic structure factors for the buffer solution and LSZ in the buffer were measured two hours after injection and are shown in Fig. 4(a). They were fitted using a three-box model using the Parratt32 software package [26] by taking the thicknesses d, the electron densities ρ, and the roughnesses σ of the three slabs as parameters. Table 1 lists the obtained parameters for LSZ in the buffer solution. The electron density profile shown in Fig. 4(b)

differs slightly from that obtained previously at the same LSZ concentration in the absence of a salt [17]. Subtracting the electron density of the buffer solution, the areas of slabs 0–2 (where the air is considered to be slab 0) and 2–3 are almost equivalent, suggesting that the adsorbed LSZ forms a double layer consisting of a densely packed first layer (slabs 0–2) above a thicker LSZ layer with a lower density (slabs 2–3).

Table 1 Structural parameters for LSZ in the buffer solution obtained by refining Fig. 4(a)

Slab number	Slab thickness d [Å]	Electron density ρ [e$^-$/Å^3]	Interface roughness σ [Å]
1	5.06	0.48	1.83
2	11.34	0.465	2.77
3	49.71	0.43	2.42
bulk		0.39	23.18

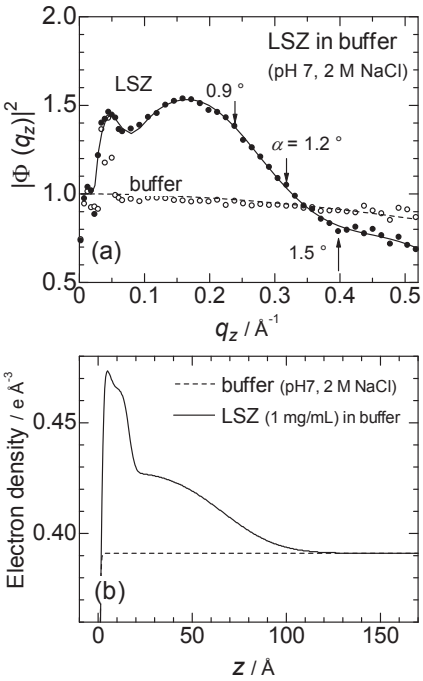

Fig. 4 (a) X-ray reflectivity profiles measured 2 hours after LSZ injection. The data were divided by the Fresnel reflectivity of the air/buffer interface. The continuous lines are the fits to the data. (b) Electron density profiles correspond to the fits to the data.

The density profiles obtained by nonlinear least-squares fitting of reflectivity curves is generally not unique. Therefore, we examined the underlying origin of the obtained x-ray reflectivity profiles to evaluate their accuracy.

The structure factor of an N-box model with sharp interfaces and uniform electron densities ρ_j and ρ_k becomes:

$$\left|\Phi(q_z)\right|^2 = \frac{1}{\rho_{\mathrm{Bulk}}^2} \times \sum_{j=0}^{N}\sum_{k=0}^{N}(\rho_{j+1}-\rho_j)(\rho_{k+1}-\rho_k)\cos\left\{q_z(z_k-z_j)\right\} \quad , (10)$$

where z_j is the depth at which the jth interface is located. The x-ray reflectivity profiles are mainly generated by the interference between the x-ray beams reflected from the interfaces having large electron density differences, $(\rho_{j+1} - \rho_j)$. Since the electron densities of the air and slab 1 differ the most in the present case, we calculated the terms with j = 0 and k = 1–3 in Eq. (10) and plotted them in Fig. 5. If the interface roughness is taken into account, the amplitudes of the cosine curves diminish at high q_z, and they fit the x-ray reflectivity profiles. The broad peak around q_z = 0.2 Å^{-1} is attributed to slabs 0–2, which correspond to the first layer of the adsorbed LSZ. The second layer (slabs 0–3) causes an additional peak in q_z < 0.1 Å^{-1}, whose amplitude is proportional to the amount adsorbed.

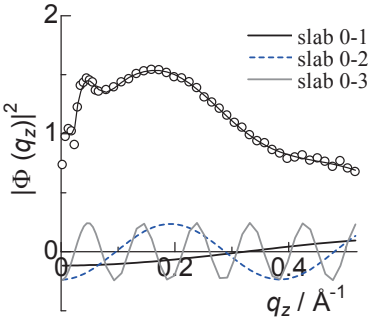

Fig. 5 Decomposition of the structure factor for x-ray reflectivity profiles measured 2 hours after LSZ injection. The data were divided by the Fresnel reflectivity of the air/buffer interface.

4.2 X-ray off-specular diffuse scattering in q_z direction

Figure 6 shows two-dimensional images of x-ray reflection peaks for x-rays incident at α = 1.5°. The intensity of off-specular diffuse scattering increased drastically after LSZ injection. A small peak, known as a Yoneda wing [27], is clearly visible at $\beta = \alpha_c$ in Fig. 6(b).

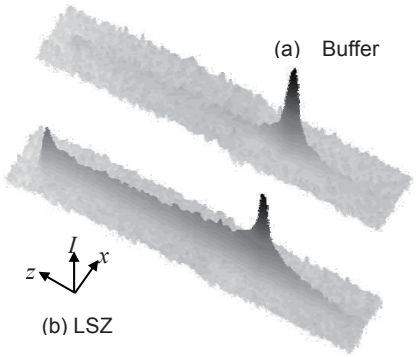

Fig. 6 Two-dimensional images of x-ray reflection peaks. (a) Buffer solution. (b) LSZ in the buffer solution measured 2 hours after injection. A small peak called the Yoneda wing at $\beta = \alpha_c$ is clearly visible.

Figure 7 shows the normalized reflection profiles of three different x-rays incident angles, which were detected without the Al attenuator. The open symbols correspond to those for the buffer solution, while the filled symbols correspond to those for LSZ in the buffer

solution measured two hours after injection. The central peaks correspond to specular reflections.

The solid and dashed curves in Fig. 7 correspond to the theoretically predicted intensities for the capillary wave (CW) model calculated using Eqs. (6) and (7) with parameters γ = 76.05 mN/m and $q_{max} \sim 2\pi/d = 2\pi/2.8$ Å^{-1} for the buffer solution, γ = 66.1 mN/m and $q_{max} = 2\pi/30$ Å^{-1} for the LSZ in the buffer solution. The intrinsic structure factor $|\Phi_0(q_z)|^2$ in Eq. (7) is calculated by a polynomial fit of the observed data shown in Fig. 4(a) in the region $q_z > 0.1$ Å^{-1}. Since the differential cross section in Eq. (7) diverges at $q_{xy} = 0$, we calculated the diffuse scattering intensities in the region $q_{xy} > 10^{-5}$ Å^{-1}. The calculated diffuse scattering intensities with the instrumental resolutions of $\Delta q_x \sim k\,\Delta(2\theta)$ and $\Delta q_y \sim k \sin(\beta)\Delta\beta$, with $\Delta(2\theta) \sim 2.3$ pixels × 0.172 mm/pixel / 538 mm and $\Delta\beta \sim 3.0$ pixels × 0.172 mm/pixel / 538 mm, which are 1.5 times larger than the FWHMs of the reflection profile at the incident angle α of 0.01°, exhibit good agreement with the observed intensities for the buffer solutions at the three different incident angles α. In contrast, the observed intensities for the LSZ in the buffer solution are much larger than the theoretically predicted intensities. This excess scattering arises from the inhomogeneity of the surface.

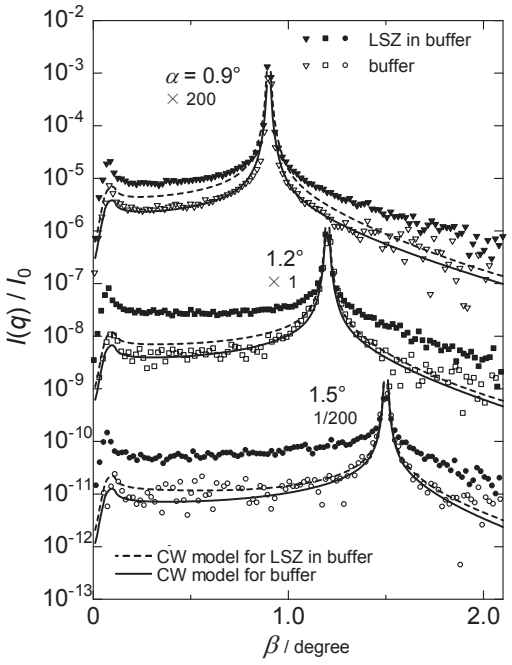

Fig. 7 Reflection profiles at α = 0.9°, 1.2°, and 1.5°. The solid curves represent the theoretical predictions based on the capillary wave model and are calculated using Eqs. (6) and (7). The observed intensities for the buffer solution (the open symbols) exhibit good agreement with those for the CW model (the solid curves), while the observed intensities for the LSZ in the buffer solution (the filled symbols) are much larger than those for the CW model (the dashed curves).

To obtain the structural parameters (i.e., the correlation length ξ and the root-mean-square roughness of the film/gas interface σ_2) of an inhomogeneous film formed on a liquid surface, Fukuto *et al*. performed the q_{xy}'-integration in Eq. (8) numerically to fit the whole pattern of the excess scattering [12,13]:

$$\left[\frac{I(q)}{I_0}\right]_{inhmg} = \frac{I(q)}{I_0} - \left[\frac{I(q)}{I_0}\right]_{hmg} \quad . \qquad (11)$$

To avoid such a complicated integration, we fitted the observed excess scattering intensities away from the specular condition with the following expression (see Appendix A1):

$$\left[\frac{I(q)}{I_0}\right]_{inhmg} \approx N\frac{e^{-\sigma_2^2 q_z^2}}{\left(1+\xi^2 q^2\right)^{\frac{3}{2}}} \quad . \qquad (12)$$

The fitting parameters are the arbitrary constant N, the correlation length ξ, and the root-mean-square roughness of the film/gas interface σ_2. Since the profile width is related to ξ, while the asymmetry of the profile is related to σ_2, these parameters can be obtained almost independently of each other.

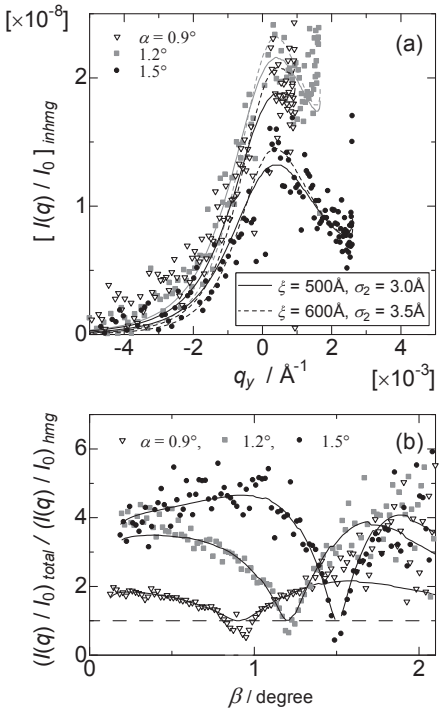

Fig. 8 (a) Excess scattering from the inhomogeneous LSZ film adsorbed by the buffer surface. The solid curves are the best fits obtained using the inhomogeneous model expressed by Eq. (12) with ξ = 500 Å and σ_2 =3.0 Å. (b) The ratio of measured intensity to the homogeneous (or CW) contribution.

The excess scattering intensities denoted by the symbols in Fig. 8(a) are obtained by subtracting the calculated intensity for the CW model from the observed intensity. The best fit with Eq. (12) is obtained when ξ = 500 Å and σ_2 =3.0 Å (the solid curves in Fig. 8) for three different x-rays incident angles α. The calculated profile with ξ = 600 Å and σ_2 =3.5 Å (denoted by the dashed curves) are also shown in Fig. 8(a) to indicate the

differences. The fit is more clearly evident in Fig. 8(b) showing the ratio of measured intensity to the homogeneous (or CW) contribution.

The estimated correlation length of ξ = 500 Å is approximately 10 times larger than the LSZ molecule, suggesting that the inhomogeneity originates from an island above the buffer surface. It is reasonable to conjecture that the LSZ molecules aggregate and form islands in the manner shown in Fig. 9. As discussed in Sec. 4.1, the x-ray reflectivity indicates that the adsorbed LSZ molecules form a double layer. It is not certain whether the whole or only the topmost double layer forms the island. However, the electron density profile shown in Fig. 4(b) differs from that obtained when no salt was present [17]. To clarify this, we need to estimate the arbitrary constant N in Eq. (12), which includes the structure factor of the inhomogeneous layer, to correlate the intrinsic structure factor derived from x-ray reflectivity measurements. This will be discussed elsewhere [28].

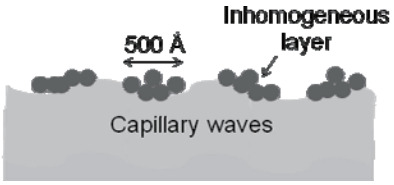

Fig. 9 Schematic model of inhomogeneous LSZ layer adsorbed at a buffer surface. The LSZ molecules aggregate to form islands above the buffer surface.

4.3 X-ray off-specular diffuse scattering in q_x direction

If the inhomogeneous layer has a particular structure in a particular direction, the scattered intensities are expected to differ in the q_x and q_y directions. Figure 10 shows the projection in the x direction of the x-ray reflection peaks shown in Fig. 6. The profiles for the buffer solution and for LSZ in the buffer solution appear to be quite similar to each other, in contrast with that in the q_y direction. The diffuse scattering produced by the surface inhomogeneity cannot be detected in the q_x direction, since the estimated effective coherence length along the surface of $1/\Delta q_x \sim 200$ Å is much smaller than that in the q_y direction of $1/\Delta q_y \sim 6300$ Å at $\alpha = 1.5°$. In addition, there is no excess scattering produced by the smaller lateral fluctuations.

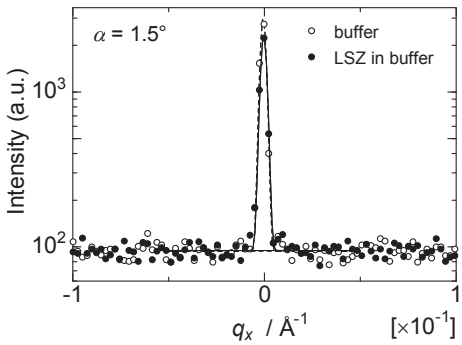

Fig. 10 x -projection of x-ray reflection peaks shown in Fig. 6. The profiles for the buffer solution and for LSZ in the buffer solution appear to be quite similar to each other.

5. CONCLUSION

We have analyzed the specular and off-specular reflection from a globular protein, LSZ, adsorbed at an air/buffer interface in the presence of a salt. The electron density profile, which differs slightly from a previous obtained result at the same LSZ concentration in the absence of a salt [17], indicates the formation of a double layer consisting of a lower-density LSZ layer beneath a densely packed top layer. The off-specular diffuse scattering from the buffer solution exhibits good agreement with the CW model. By contrast, that from LSZ in the buffer solution measured two hours after injection is higher than predicted. We proposed a simple formula to describe the excess scattering intensity. The formula fitted the excess scattering at different incident angles with a correlation length ξ of 500 Å and the root-mean-square roughness of the film/gas interface σ_2 of 3.0 Å, suggesting that the LSZ molecules aggregate to form islands with diameters of about 500 Å above the buffer surface. The excess scattering produced by the surface inhomogeneity was not observed in the q_x direction, since the estimated effective coherence length along the surface of $1/\Delta q_x \sim 200$ Å is much shorter than the correlation length of the inhomogeneous layer.

The PILATUS detector accurately obtains the full range of x-ray specular and off-specular reflections in an extremely short time (1 s), allowing the out-of-plane and in-plane structures of a biological system at an interface to be determined for the first time.

ACKNOWLEDGEMENTS

The authors are grateful for helpful discussions with Professor Peter Pershan of Harvard University (see Appendix A2) and Emeritus Professor Takao Iijima of Gakushuin University. The synchrotron radiation experiments were performed at the BL37XU in the SPring-8 facility with the approval of the Japan Synchrotron Radiation Research Institute (JASRI) (Proposal No. 2009A1686).

APPENDIX

A1 Derivation of Eq. (12)

In a previous study, Fukuto *et al*. performed the q_{xy}'-integration in Eq. (8) numerically to fit the whole pattern of the excess scattering to obtain the parameters ξ and σ_2 [12,13]. To avoid such a complicated integration, we propose a simple formula to describe the excess scattering intensity.

In the previous study, the electron density normal to the surface for the inhomogeneous film $\phi_2 \cdot \rho_{\mathrm{Bulk}}$ was assumed to be constant [12,13]. In contrast, in the present study, the electron density varies with z (see Sec. 4.1). Therefore, we used Eq. (8)′ instead of Eq. (8)

$$\frac{1}{A_0}\left(\frac{d\sigma}{d\Omega}\right)_{inhmg} \approx \frac{1}{16\pi^2}\left(\frac{q_c}{2}\right)^4 \frac{e^{-\sigma_2^2 q_z^2}}{q_z^2 \sin(\alpha)}\left|\Phi_2(q_z)\right|^2 \times \frac{1}{(2\pi)^2}\int_{q'_{xy}\le q_{\max}} d^2\mathbf{q}'_{xy}\, \frac{2\pi\eta}{q'^2_{xy}}\left(\frac{q'_{xy}}{q_{\max}}\right)^{\eta} C_2\left(\mathbf{q}_{xy}-\mathbf{q}'_{xy}\right)$$

with

$$\left|\Phi_2(q_z)\right|^2 = \left|\frac{1}{\rho^{Bulk}}\int dz\, \frac{\partial\langle\rho(z)\rangle_{xy}}{\partial z}\, e^{iq_z z}\right|^2 . \qquad (8)'$$

Furthermore, the asymptotic decay $1/q'^{2-\eta}_{xy}$ in the q_{xy}'-integration can be roughly approximated with a delta function $\delta(q_{xy}')$ to give:

$$\frac{1}{A_0}\left(\frac{d\sigma}{d\Omega}\right)_{inhmg} \approx \frac{1}{16\pi^2}\left(\frac{q_c}{2}\right)^4 \frac{e^{-\sigma_2^2 q_z^2}}{q_z^2 \sin(\alpha)}\left|\Phi_2(q_z)\right|^2 \quad , \\ \times \frac{N'}{(2\pi)^2}\int_{q'_{xy}\le q_{\max}} d^2\mathbf{q}'_{xy}\, 2\pi\eta\, \delta(\mathbf{q}'_{xy}) C_2(\mathbf{q}_{xy}-\mathbf{q}'_{xy}) \qquad (8)''$$

where N' is a factor generated by this approximation.

Except for the region close to the specular condition, the scattering intensity profile is not greatly affected by the instrumental resolution function. Thus, the instrumental resolution function Ξ can be replaced by a delta function $\delta(q_{xy} - q_{xy}')$:

$$\Xi_q(q_{xy}-q'_{xy}) = \delta(q_{xy}-q'_{xy}) \qquad \text{if } \left|q_{xy}\right| >> 0 \quad . \qquad (13)$$

Using Eqs. (6), (8)″, (9), and (13), we obtain the excess scattering intensity:

$$\left[\frac{I(q)}{I_0}\right]_{inhmg} \approx N\frac{e^{-\sigma_2^2 q_z^2}}{\left(1+\xi^2 q^2\right)^{\frac{3}{2}}} \quad . \qquad (12)$$

In spite of the rough approximations used, Eq. (12) describes the excess scattering very well, as shown in Fig. 8.

A2 Reply to Prof. Pershan's comments

Below are several helpful comments given by Professor Peter Pershan who has conducted a lot of pioneering work on liquid surfaces and our responses to them.

(1) Importance of defining the instrumental resolution when estimating the correlation length of inhomogeneities

"There is a fundamental problem in trying to separate the effects of surface inhomogeneities from capillary roughness that I would like to try to explain.

In principle if one had infinitely fine resolution the capillary wave scattering for your model of the surface would lead to an intense/sharp peak at $q_{xy} = 0$ that would dominate any of the excess scattering due to surface inhomogenieties. This occurs because if gravity is neglected the amplitude of the capillary peak is an infinitely high singularity while the surface inhomogeneities have a finite width/finite amplitude. As the resolution becomes coarser the singular capillary peak broadens and the intensity of the scattering due to the inhomogeneities increases. At the point that the resolution becomes comparable to the correlation length of the inhomogeneities it becomes hard to distinguish between these two signals. One way this can sometimes be done is to compare the FWHM of the diffuse profile (your Fig. 6) with the FWHM of the direct beam. For a flat surface in which the capillary waves dominate the diffuse scattering the FWHM width of the profile should be comparable to the resolution determined width of the direct beam. Is this true for you measurement?

On the other hand, if $1/\xi$ is comparable to, or smaller than, the resolution the two signals can not easily be separated. One possible way for large η (i.e. for large $(k_BT/2\pi\gamma)\, q_z^2$) is that for large $q_{x,y}$ the tails of the diffuse scattering do become larger than the correlation determined tails of the inhomogeneities (i.e. your Eq. 9 or 12) and that might be a good signature if you really know the shape of the inhomgeneity induced scattering and can show that the measured diffuse scattering is dominated by the capillary form. This leads me to comparing your Fig. 6 to Fig. 4 in Masa's 1998 PRL [12]. Note that for Masa's figure the diffuse scattering at $\beta = \alpha$ is the same for the homogeneous/inhomogeneous surfaces. This means that that the specular condition the scattering for the inhomogeneous surface is dominated by the singular peak in the capillary spectrum. Masa could be certain of this because he reports measurements of the difference $\Delta I = I(\theta = 0) - I(\delta\theta)$ that is defined in the second column of Masa's 1998 PRL So long as $1/\xi$ > the resolution the excess scattering at $\beta = \alpha$ makes no contribution to ΔI and his Fig. 4 is just the excess. I don't know if you can do this with your data."

– Unfortunately, we don't have the direct beam profile to compare with the diffuse scattering profile. However, as Fig. 7 shows, the shape of the diffuse scattering profile close to the specular region exhibits very good agreement with that predicted by the capillary wave (CW) model with an instrumental resolution estimated from the FWHMs of the reflection profile at the incident angle α of 0.01°. Furthermore, the effective coherence length along the surface of $1/\Delta q_y \sim 6300$ Å at $\alpha = 1.5°$ is much larger than the correlation length ξ of 500 Å for the inhomogeneous layer, allowing the excess scattering to be separated from the CW contribution in the present case. Figure 8(b) shows the ratio of our measured intensity to the homogeneous (or CW) contribution in accordance with Masa's Fig. 4 in 1998 PRL [12]. The intensities at $\beta = \alpha$ deviate slightly from unity, which might be caused by an error in the estimated instrumental resolution or intrinsic structure factor $\left|\Phi_0(q_z)\right|^2$. However, in contrast with Masa's case, our $1/\xi$ is much larger than the resolution described above. Furthermore, the diffuse scattering intensity from our inhomogeneous layer is much larger than the CW contribution out of the specular region, as shown in Fig. 7 and 8(b). We consider, therefore, that we do not have to treat our data in the strict manner that Masa did and that we can estimate the correlation length ξ outside the specular region using the simple formula proposed in this paper.

(2) Background subtraction

"When you subtract the background this way (See 2.2) you can also be subtracting a contribution from the capillary waves at small q_y. When we do something like this the theoretical model that we use is the difference between the capillary theory for the two signals."

– We think we do not have to consider the CW contribution in the background subtraction even though we took a point very close to the specular region ($q_x \sim 0.012$ Å^{-1}) as the background. As shown in Fig. 10, the intensity outside of the specular region is almost constant because of the scattering from the x-ray windows, the bulk liquid, etc., which become much

larger than the CW contribution when no receiving slit is present.

(3) Formula describing the capillary wave model

"I don't use the Sanyal formula [6]. But, as I wrote in the article in P. S. Pershan, "X-ray Scattering From Liquid Surfaces: Effect of Resolution", Journal of Physical Chemistry B 113, 3639 (2009) [20], the Sanyal formula is OK for reflectivity if η is less than one. On the other hand, you can not use it if you want to subtract the out of the plane diffuse scattering since it assumes an infinitely wide resolution. You say that you do subtract background but the theory that you compare the background subtracted data with does not include this effect."

– We used Sanyal's formula in the first draft and a previous paper [15], because this formula can describe both the specular and off-specular reflection profiles using a single equation. As you pointed out, however, this formula which has a $q_y^{\eta-1}$ shape instead of $q_{xy}^{\eta-2}$ as a result integrating in the q_x direction, which does not fit the present case very well in which the resolution in the q_x direction is only several tens of times coarser than that in the q_y direction. In the revised paper, we recalculated the diffuse scattering using Eqs. (6) and (7) instead of using Sanyal's formula.

Figure A1 shows an example of the theoretical prediction for the CW model calculated using Eqs. (6) and (7), compared with that calculated using Sanyal's formula. In the specular region and the large β region, Eqs. (6) and (7) fit the observed intensity much better than Sanyal's formula.

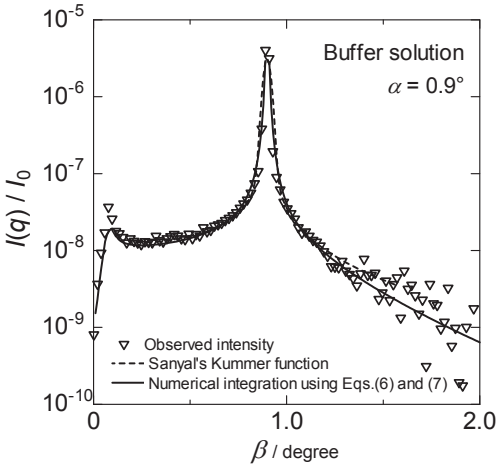

Fig. A1 Reflection profiles for the buffer solution at $\alpha = 0.9°$. The theoretical predictions for the CW model are calculated using Eqs. (6) and (7) (the solid curve is the same curve shown in Fig. 7), and Sanyal's formula (dashed curve).

REFERENCES

[1] M. Tolan: "X-Ray Scattering from Soft-Matter Thin Films", Springer (1999), pp113-149.
[2] F. P. Buff, R. A. Lovett and F. H. Stillinger, *Phys. Rev. Lett*. **15**, 621-623 (1965).
[3] S. K. Sinha, E. B. Sirota, S. Gasoff, and E. B. Stanley, *Phys. Rev. B***38**, 2297-2311 (1988).
[4] A. Braslau, M. Deutsch, P. S. Pershan, A. H. Weiss, J. Als-Nielsen and J. Bohr, *Phys. Rev. Lett*. **54**, 114-117 (1985).
[5] D. K. Schwartz, M. L. Schlossman, E. H. Kawamoto, G. J. Kellogg, P. S. Pershan and B. M. Ocko, *Phys. Rev. A***41**, 5687-5690 (1990).
[6] M. K. Sanyal, S. K. Sinha, K. G. Huang, and B. M. Ocko, *Phys. Rev. Lett*. **66**, 628-631 (1991).
[7] P. S. Pershan, *Colloids Surface A***171**, 149-157 (2000).
[8] O. Shpyrko, M. Fukuto, P. S. Pershan, B. Ocko, I. Kuzmenko, T. Gog, and M. Deutsch, *Phys. Rev. B***69**, 245423 (2004).
[9] H. Tostmann, E. DiMasi, P. S. Pershan, B. M. Ocko, O. G. Shpyrko, and M. Deutsch, *Phys. Rev. B***59**, 783-791 (1999).
[10] O. Shpyrko, P. Huber, A. Grigoriev, P. S. Pershan, B. Ocko, H. Tostmann and M. Deutsch, *Phys. Rev. B***67**, 115405 (2003).
[11] Z. Li. Zhao, J. Quinn, M. H. Rafailovich, J. Sokolov, R. B. Lennox, A. Eisenberg, X. Z. Wu, M. W. Kim, S. K. Sinha, and M. Tolan, *Langmuir*, **11**, 4785-4792 (1995).
[12] M. Fukuto, R. K. Heilmann, P. S. Pershan, J. A. Griffiths, S. M. Yu, and D. A. Tirrell, *Phys. Rev. Lett*. **81**, 3455 -3458 (1998).
[13] M. Fukuto, R. K. Heilmann, P. S. Pershan, S. M. Yu, J. A. Griffiths, and D. A. Tirrell, *J. Chem. Phys*. **111**, 9761-9777 (1999).
[14] M. Fukuto, R. K. Heilmann, P. S. Pershan, A. Badia, and R. B. Lennox, *J. Chem. Phys*. **120**, 3446-3459 (2004).
[15] Y. F. Yano, T. Uruga, H. Tanida, H. Toyokawa, Y. Terada, and M. Takagaki, *J. Phys. Conf. Ser*. **83**, 012024 (2007).
[16] Y. F. Yano, T. Uruga, H. Tanida, H. Toyokawa, Y. Terada, M. Takagaki, and H. Yamada, *Eur. Phys. Special Topics*, **167**, 101-105 (2009).
[17] Y. F. Yano, T. Uruga, H. Tanida, H. Toyokawa, Y. Terada, M. Takagaki, and H. Yamada, *Langmuir*, **25**, 32-35 (2009).
[18] http://pilatus.web.psi.ch/pilatus.htm
[19] P. Kraft, A. Bergamaschi, Ch. Broennimann, R. Dinapoli, E. F. Eikenberry, B. Henrich, I. Johnson, A. Mozzanica, C. M. Schlepütz, P. R. Willmott and B. Schmitt, *J. Synchrotron Rad*. **16**, 368-375 (2009).
[20] P. S. Pershan, *J. Phys. Chem. B***113**, 3639-3646 (2009).
[21] D. E.Graham, and M. C. Phillips, *J. Colloid Interface Sci*. **70**, 403-414 (1979).
[22] B. C. Tripp, J. J. Magda, and J. D. Andrade, *J. Colloid Interface Sci*. **173**, 16-27 (1995).
[23] M. D. Lad, F. J. Birembaut, M. Matthew, R. A. Frazier, and R. J. Green, *Phys. Chem. Chem. Phys*. **8**, 2179-2186 (2006).
[24] J. R. Lu, T. J. Su, R. K. Thomas, and J Penfold, J. Webster, *J. Chem. Soc. Faraday Trans*. **94**, 3279-3287 (1998).
[25] C. Postel, O. Abillon, and B. Desbat, *J. Colloid Interface Sci.* **266**, 74-81 (2003).
[26] This Reflectivity software is available from: <http://www.hmi.de/bensc/instrumentation/instrumente/v6/refl/parratt_en.htm>.
[27] Y. Yoneda, *Phys. Rev.* **131**, 2010 -2013 (1963).
[28] Y. F. Yano, T. Uruga, H. Tanida, H. Toyokawa, Y. Terada, M. Takagaki, and H. Yamada, in preparation.

(Received July 14, 2009;Accepted Septembe 17, 2009)